Developmental Cell
Article

Symmetry Breaking in Spore Germination Relies on an Interplay between Polar Cap Stability and Spore Wall Mechanics

Daria Bonazzi,[1,2,6] Jean-Daniel Julien,[3,4,5,6] Maryse Romao,[2] Rima Seddiki,[1] Matthieu Piel,[2] Arezki Boudaoud,[3,5,*] and Nicolas Minc[1,*]
[1]Institut Jacques Monod, 15 rue Hélène Brion, 75205 Paris Cedex 13, France
[2]Institut Curie, UMR 144 CNRS/IC, 26 rue d'Ulm, 75248 Paris Cedex 05, France
[3]Laboratoire Joliot-Curie, CNRS, ENS de Lyon, Université de Lyon, 46 Allée d'Italie, 69364 Lyon Cedex 07, France
[4]Laboratoire de Physique, CNRS, ENS de Lyon, UCBL Lyon I, 46 Allée d'Italie, 69364 Lyon Cedex 07, France
[5]Reproduction et Développement des Plantes, INRA, CNRS, ENS de Lyon, UCBL Lyon I, 46 Allée d'Italie, 69364 Lyon Cedex 07, France
[6]These authors contributed equally to this work
*Correspondence: arezki.boudaoud@ens-lyon.fr (A.B.), minc@ijm.univ-paris-diderot.fr (N.M.)
http://dx.doi.org/10.1016/j.devcel.2014.01.023

SUMMARY

The morphogenesis of single cells depends on their ability to coordinate surface mechanics and polarity. During germination, spores of many species develop a polar tube that hatches out of a rigid outer spore wall (OSW) in a process termed outgrowth. However, how these awakening cells reorganize to stabilize this first growth axis remains unknown. Here, using quantitative experiments and modeling, we reveal the mechanisms underlying outgrowth in fission yeast. We find that, following an isotropic growth phase during which a single polarity cap wanders around the surface, outgrowth occurs when spores have doubled their volume, concomitantly with the stabilization of the cap and a singular rupture in the OSW. This rupture happens when OSW mechanical stress exceeds a threshold, releases the constraints of the OSW on growth, and stabilizes polarity. Thus, outgrowth exemplifies a self-organizing morphogenetic process in which reinforcements between growth and polarity coordinate mechanics and internal organization.

INTRODUCTION

Organisms ranging from bacteria to fungi and plants can produce spores. These are dehydrated cells adapted for survival in harsh environments over very long periods of time ranging from weeks to thousands of years in some bacteria (Cano and Borucki, 1995; McKenney et al., 2013; Neiman, 2005). Spore resistance is associated with a rigid protective extracellular shell deposited at sporulation, called the outer spore wall (OSW) or spore coat (Arellano et al., 2000; García et al., 2006; Klobutcher et al., 2006; Wallace et al., 2011). Once conditions are favorable, spores germinate to exit dormancy, resume growth, and develop a single polarized tube that hatches out of the OSW, in a process termed outgrowth (Hatanaka and Shimoda, 2001; Kono et al., 2005; Pandey et al., 2013). Because of its particular cell cycle, de novo protein synthesis, and exit from prolonged period of dormancy, outgrowth poses an outstanding morphogenetic puzzle, which is to understand how these awakening symmetric cells may reorganize their interior to stabilize their very first polarized growth axis.

Polarized growth involves the formation of cortical polar caps of the GTP-bound form of a GTPase, such as Cdc42p in yeast (Drubin, 1991). These caps may be spatially stabilized by extrinsic cues, or can self-assemble at random positions by positive feedback (Drubin, 1991; Howell et al., 2012; Wedlich-Soldner et al., 2003; Wu and Lew, 2013). Yet, it becomes increasingly clear that mechanisms regulating cap establishment and/or stabilization may largely vary between different periods of cellular life cycles, even in a single given organism (Bendezú and Martin, 2013; Das et al., 2012; Dyer et al., 2013; Wu and Lew, 2013). In yeast and fungal cells, polar caps serve as platforms to direct local membrane addition and cell-wall remodeling, needed for surface expansion (Chang and Martin, 2009; Drubin, 1991). Growth itself involves mechanical work from high internal osmotic pressure that allows deforming newly synthesized cell wall (Bastmeyer et al., 2002; Boudaoud, 2003; Minc et al., 2009a). Thus, the morphogenesis of these single cells ultimately relies on an integration of biochemical and biomechanical signals (Harold, 1990; Slaughter and Li, 2006).

Here, we use quantitative time-lapse microscopy to understand how single spores break symmetry to become rod shaped in the model fission yeast *Schizosaccharomyces pombe*. We show that germination is followed by a long period of near-isotropic growth during which a single polar cap of active-cdc42p wanders around and drives small local growth sites that fail to progress, disassemble, and reform at a new position. We demonstrate that this unstable behavior is associated with the presence of the rigid OSW, which acts as a mechanical barrier that hinders growth and destabilizes polarity, and that cap stabilization occurs at outgrowth when the OSW ruptures. We develop a computational model that fully reproduces spore development in silico. This work demonstrates that the switch in polar cap stability at outgrowth can be explained by a simple positive-feedback loop between growth and polar cap stabilization.

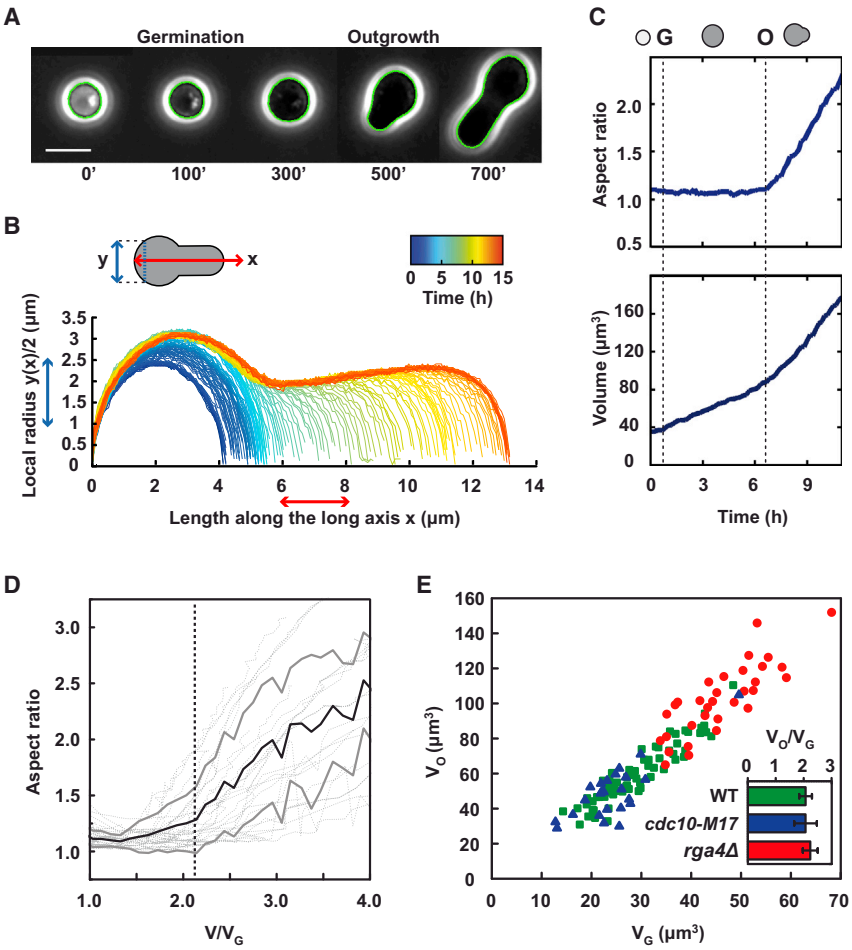

Figure 1. Spore Outgrowth Onset Correlates with a Robust Size-Increase Threshold

(A) Phase-contrast time-lapse superimposed with automated shape contour detection of a wild-type fission yeast spore germinating and outgrowing.

(B) Morphogenetic plot representing the temporal evolution of cell morphogenesis.

(C) Evolution of single-cell aspect ratio and volume as a function of time.

(D) Integrated morphogenesis at the population level (n = 25 spores). The black line depicts the averaged cell aspect ratio as a function of the averaged cell volume normalized with the volume at germination. Thick gray lines delimit the SD, and thin gray lines are plots arising from individual spore morphogenesis tracking.

(E) Volume at the onset of outgrowth, V_0 plotted as a function of the volume at germination, V_G. These volumes are measured from time-lapse phase images. The onset of outgrowth is defined as the inflexion point of the aspect ratio curve. Green, blue, and red data points, respectively, correspond to single WT, *cdc10-M17* at restrictive temperature (37°C), and *rga4Δ* spores. Error bars represent SDs. Scale bars, 5 µm. See also Figure S1 and Movies S1 and S2.

RESULTS

The Developmental Morphogenesis of Single Fission Yeast Cells

We quantitated the morphogenetic development of single fission yeast spores by performing long (over 10 hr) time-lapse phase-contrast microscopy with frequencies down to 5 min (Figure 1A; Movie S1 available online). Spores were rapidly transferred from starvation media to agar pad containing rich media. Phase contrast allowed delineating germination onset, which is characterized by a bright-phase to dark-phase transition (Figure S1A) (Hatanaka and Shimoda, 2001). Spores then grew in a near-isotropic manner for about 6–8 hr and entered outgrowth, which corresponds to the definition and stabilization of the first polarized growth axis characterizing the rod-shaped fission yeast cell (Hatanaka and Shimoda, 2001) (Figure 1A). The cells then kept on growing for another 3–4 hr before entering mitosis. Outgrowing cells kept their bottle-like shape and remained monopolar, growing away from the spore body for several cell cycles (Movie S2). Phase images were segmented and analyzed to quantitate single spore dimensions, aspect ratios, and volumetric growth rates (Figures 1B–1D; Experimental Procedures). At outgrowth, the aspect ratio depicted a sharp increase, which marked the extension of the polarized tube, and single-cell growth rates also increased abruptly by a factor of 2.4 ± 0.4 on average (Figure S1B).

Outgrowth Onset Is Associated with a Robust Fold Change in Cell Size

We used this approach to investigate whether outgrowth could correlate with an internal timer, a size increase, or a specific spore size (Mitchison and Nurse, 1985). The absolute time from germination to outgrowth depicted cell-to-cell variation of around 30% in the same field of observation. Not surprisingly, this timing was also largely dependent on temperature, humidity, as well as strain background (data not shown). We thus used cell volume as an indicator of spore developmental progression, to generate an averaged morphogenetic development at the cell population level (Figure 1D). This analysis revealed that the onset of outgrowth correlated with a fixed spore volume increase. We thus computed the volume at germination (V_G) and at the onset of outgrowth (V_O) for individual spores. This showed that the volume at outgrowth can vary up to 3- to 4-fold in a wild-type (WT) population and revealed a linear scaling between V_O and V_G (R^2 = 0.87) with a slope of 2.07 ± 0.12 (n = 67). This scaling was similar in spores with larger initial volumes like those produced by the fat mutant *rga4Δ* (volume ratio, $< V_O/V_G > =$ 2.22 ± 0.13, n = 32) (Figure 1E) (Das et al., 2007; Tatebe et al., 2008). This size increase was also independent on G1/S cell-cycle transition, which is known to occur around these stages of spore development (Hatanaka and Shimoda, 2001; Mitchison and Nurse, 1985), as spores of the *cdc10-M17* mutant, which arrest in G1 at restrictive temperature (Nurse et al., 1976), depicted similar volume ratios ($<V_O/V_G> = 2.07 \pm 0.20$, n = 23) (Figures 1E, S1C, and S1D). Thus, outgrowth correlates with spore

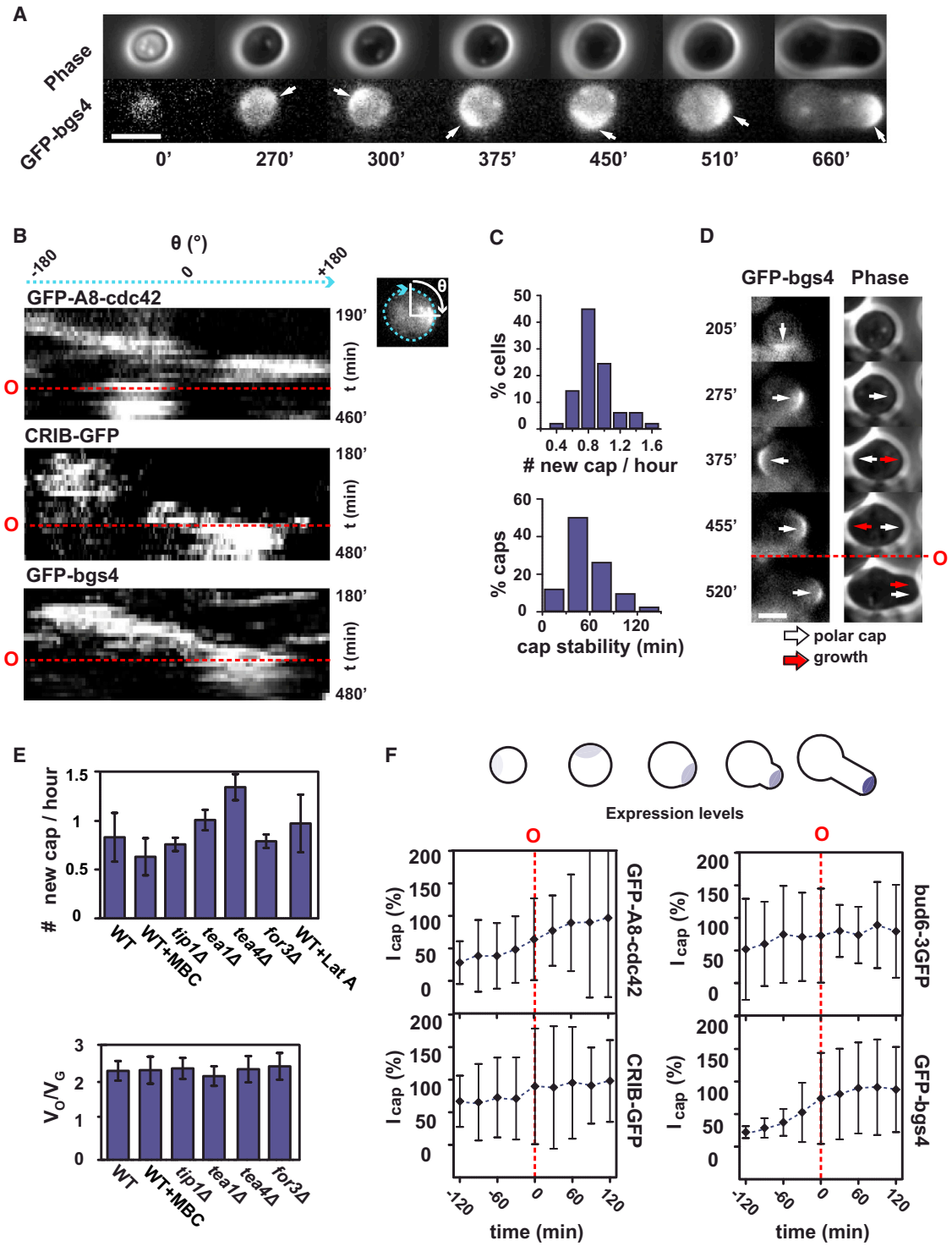

Figure 2. A Polarity Cap Wanders around the Symmetric Spore and Finally Stabilizes to Promote Outgrowth

(A) Time-lapse phase-contrast and epifluorescence images of a developing spore expressing the polarized growth marker GFP-bgs4. White arrows point at newly assembled caps.

(B) Cell kymographs representing the changes of localization over time of the polarity factors GFP-A8-cdc42, CRIB-GFP (a marker for active GTP-cdc42), and GFP-bgs4. Kymographs for GFP-bgs4 and GFP-A8-cdc42 are computed from epifluorescence time lapse, whereas those for CRIB-GFP are computed from confocal single midslices.

(C) Quantification of polar cap frequency and stability in time (n = 50 spores). A new polar cap is defined as a newly assembled cap at a different location than the previous one. Final stable outgrowth caps are not counted. Cap stability corresponds to the time between assembly and disassembly.

(legend continued on next page)

volume doubling, independently of absolute size or cell-cycle progression.

A Wandering Polar Cap Becomes Stable at Outgrowth

To understand polarity establishment and stabilization in spores, we then imaged fluorescently tagged canonical polarity markers throughout spore development. For polarized growth, vegetative fission yeast cells assemble clusters of polarity proteins into a polar cap at their growing tips (Chang and Martin, 2009). This cluster includes the small GTPase cdc42p, actin regulators, and cell-wall remodeling factors, which promote tip growth. We followed the localization of GFP-tagged cdc42p (Rincón et al., 2009) and its active GTP-bound form using the CRIB-GFP fusion (Tatebe et al., 2008), the actin-associated marker bud6-3GFP (Glynn et al., 2001) and the membrane glucan synthase GFP-bsg4, which marks sites of cell-wall synthesis (Cortés et al., 2005). Strikingly, all these factors assembled into a single cap long before outgrowth (first visible between 1 and 3 hr after germination), which disassembled and reassembled at successive locations, yielding a stochastic wandering motion around the spore surface, and finally stabilized to promote outgrowth (Figures 2A, 2B, S2A, and S2B; Movie S3). In some cases, the polar cap completely disassembled to reform at a new location, whereas, in other cases, the cap displayed local sliding or rearrangement in a restricted area of the spore surface (Movie S3). This unstable behavior was reminiscent of oscillating states of polarity in budding yeast, vegetative fission yeast, and in adherent mammalian cells (Bendezú and Martin, 2012, 2013; Das et al., 2012; Fink et al., 2011; Howell et al., 2012; Wedlich-Soldner et al., 2003). However, in these spores, a large fraction of caps appeared to be stable for a comparatively longer time period (ranging from 30 to 90 min) (Figure 2C). This yielded an average frequency of about 0.75 newly assembled caps per hour and a total of three to four transient unstable caps visible in the plane of focus between germination and outgrowth. We did not note dampening of cap wandering behavior before stabilization. Rather, the transition between wandering and definitive docking of the cap appeared to be abrupt in most cases (Figures 2B and S2A).

Importantly, all these polarity components colocalized two by two, and cowandered together (Figure S2C). In addition, transient cap formation led in ~65% of cases to small localized growth sites that extended out of the rounded spore and failed to progress (Figure 2D; Movie S4). Local growth followed the assembly of a new GFP-bgs4 polar cap with a time delay ranging from 5 to 20 min typically (Figure 2D; Movie S4). Thus, the upstream polarity machinery appears to be properly assembled and competent for polar growth soon after germination, but destabilizing elements may hinder polarity maintenance until the spore has increased its volume sufficiently.

Cap Stabilization Does Not Involve NETO Factors, Memory Cues, or Polarity Protein Levels

We next tested if elements that spatially stabilize polarity in vegetative cells could contribute to cap maintenance at outgrowth. One class of such characterized factors are those that promote polarity establishment at the new end (NETO, New End Take Off) in vegetative cells, such as microtubules (MTs) and MT + TIP factors (Chang and Martin, 2009). MTs in spores were short and disorganized until after outgrowth, and treatment with a microtubule-inhibitory drug (MBC), which blocks MT polymerization in spores and cells neither blocked wandering nor altered volume-doubling required for stabilization. In addition, mutants in MT-based polarity pathways defined by tip1p, tea1p, and tea4p and mutants defective in actin cables assembly such as in the formin for3p all showed similar behavior as WT (Figures 2E, S3A, S3C, and S3E). Complete depolymerization of actin with Latrunculin A halted spore growth but did not block wandering, as seen in other cell types exhibiting polarity oscillations (Figures 2E, S3B, and S3D) (Howell et al., 2012).

Cap stabilization did not appear to involve fixed spatial cues in the spore (Chang and Martin, 2009; Drubin, 1991). Spores that remained attached to each other assuming the shape of the mother ascus outgrew along an axis independent of the previous meiotic division axis (Figure S3F; Movie S5). Additionally, in a subset of time lapses we saw the polar cap exploring several times the incipient site of outgrowth, before stabilizing (see Movie S4, for an example). These data suggest that outgrowth involves different polarity stabilizing elements than in vegetative cells.

We also quantified the concentration of these polarity factors in the cap with confocal microscopy, to test a hypothesis in which polarity proteins that are being de novo synthesized in spores may need to reach a saturating level to stabilize. This showed that the expression levels were noisy with 5- to 10-fold variations in protein concentration at the cap between different spores at a given time, so that some outgrowing spores could display concentrations lower than spores at earlier stages. Also, the overall increase in expression did not obviously saturate at outgrowth and continued to rise until the first mitosis (Figure 2F). Although these data do not rule out the existence of a concentration threshold in an uncharacterized cytoplasmic factor that may stabilize the cap, they do not support a cap maturation model needed for stabilization.

The Outer Spore Wall Encases the Spore and Displays a Singular Rupture at Outgrowth

We thus turned our attention to factors that are specific to this spore-to-cell transition. One specific feature of spores is the encasing OSW. The fission yeast OSW is deposited onto the inner cell wall during sporulation, and is also composed of polysaccharides, but it features different crosslinking and the

(D) Time-lapse phase-contrast and fluorescence images of GFP-bgs4 cap wandering and corresponding local growth site.
(E) Frequency of newly assembled successive GFP-bgs4 polar caps, in the indicated conditions and mutants, and corresponding outgrowth volume ratio V_0/V_G ($n > 25$ spores for each condition).
(F) Quantification of changes in fluorescence levels of different polarity factors (see Experimental Procedures): GFP-A8-cdc42, CRIB-GFP, bud6-3GFP, and GFP-bgs4 from 2 hr before to 2 hr after outgrowth ($n > 10$ spores for each marker). Error bars represent SDs.
Scale bars, 5 μm. See also Figures S2 and S3 and Movies S3 and S4.

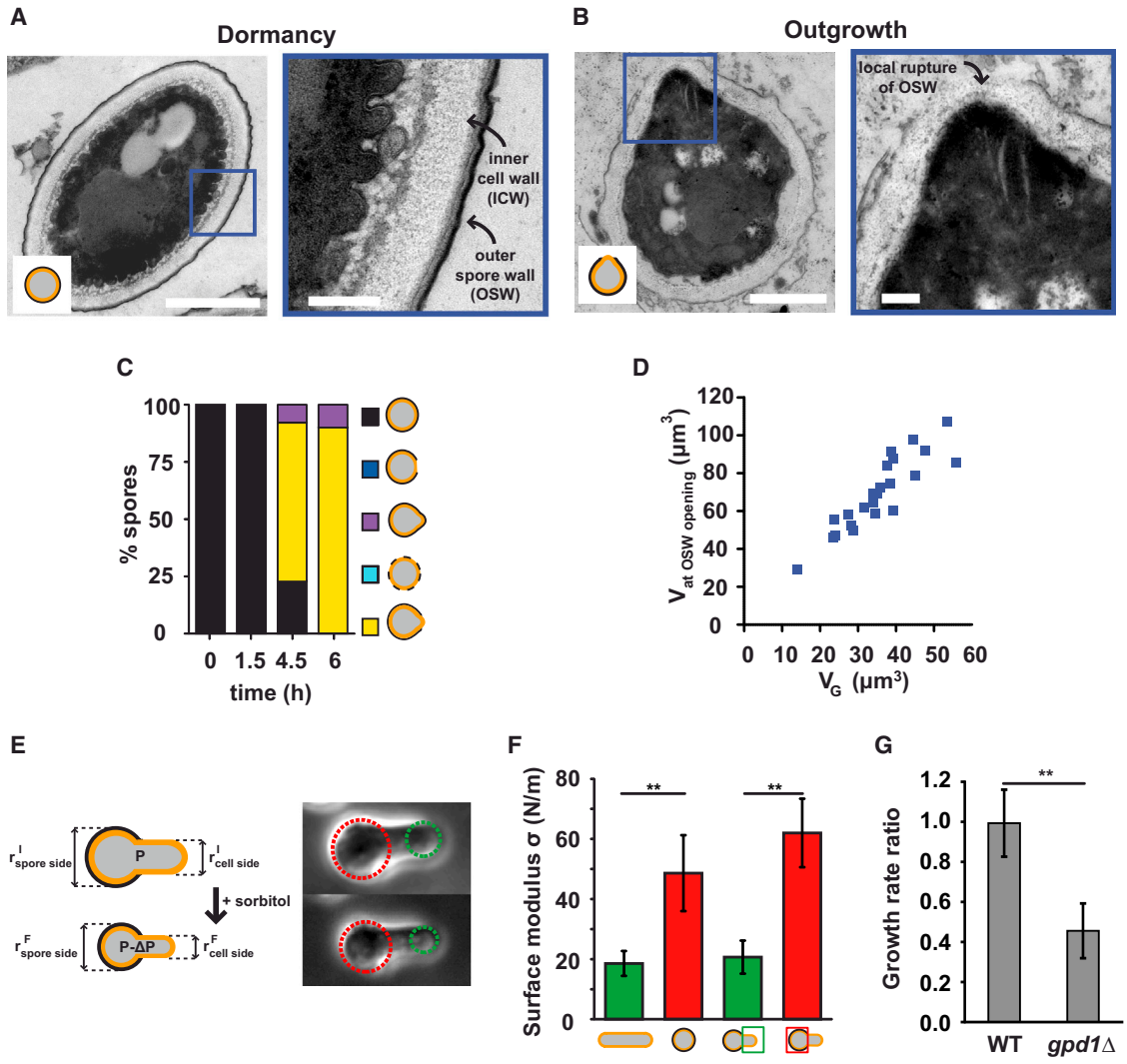

Figure 3. The Outer Spore Wall Is Rigid and Displays a Singular Rupture at the Time and Location of Outgrowth

(A) Transmission electron microscopy picture of a dormant spore and corresponding close-up view on OSW.

(B) Outgrowing spore after 6 hr of incubation at 30°C and corresponding close-up view on the outgrowth site, which displays a local rupture in the OSW (scale bars in large view, 1 μm; and in close-ups, 200 nm).

(C) Quantification of the phenotypes of outer wall rupture at different times from germination (n = 52 spores).

(D) Volume at the moment of OSW rupture, as assayed by growing spores in medium supplemented with an inner/vegetative cell-wall digestion mix, plotted as a function of the volume at germination for WT spores.

(E) Stress-strain approach used to measure the elastic properties of the inner and outer wall.

(F) Cell-wall surface moduli for vegetative cells, spores, and the two sides of an outgrown spore (n > 10 cells or spores).

(G) Ratio between growth rate before and after treatment with sorbitol measured in WT and *gpd1Δ* spores (n = 7 spores for each condition). Error bars represent SDs.

**p < 0.01, Student's t test. See also Figure S3.

presence of chitin, both of which may confer atypical properties that allow this layer to protect spores from harsh environment (Arellano et al., 2000; García et al., 2006; Tanaka and Hirata, 1982). We visualized the OSW at gradual time intervals using transmission electron microscopy (TEM). In dormant spores, the OSW was visible as a homogeneous electron-dense multilayered structure, about 15–20 nm thick. This thickness remained nearly constant throughout development (data not shown). Yet, we noted that the OSW often appeared wrinkled at early stages and flatter at later stages (Figures 3A and S4A), suggesting that these wrinkles may unfold as a result of spore growth, without drastic remodeling of the OSW.

Interestingly, at timing corresponding to outgrowth, we observed a local rupture/dissolution of the OSW at the site of tip emergence (Figures 3B, 3C, and S4A). Rupture of the wall was only obvious in spores with an outgrowing tip, and we did not note major opening at earlier time points, or at sites away from the growth zone. At later time points, the OSW appeared

to remain intact at the back of the outgrown cell (Figure S4A). By contrast, the inner cell wall appeared to be continuous with the emerging vegetative cell wall. To monitor the opening of the OSW in live spores, we grew spores in medium supplemented with an inner/vegetative wall digestion enzyme mix, which rapidly causes the death of outgrown spores and vegetative cells but does not affect spores protected by an intact OSW (Figure S4B). Spores developed normally in the enzyme mix and abruptly died at a volume ratio of $< V_{OSW\ opening}/V_G > = 1.97 \pm 0.22$ (n = 24) (Figures 3D and S4B), suggesting that the OSW opens when spores have doubled their volume. Thus, outgrowth is concomitant with a singular rupture in the OSW at the site of polar tube emergence.

The Outer Spore Wall Is Very Stiff and May Hinder Growth

To understand how the OSW may influence spore development, and how it may rupture at outgrowth, we assessed its mechanical properties using cellular stress-strain experiments (Figures 3E and S4C). This assay consists in applying a dose-dependent negative osmotic pressure by rinsing cells placed in microfluidic chambers with different concentrations of sorbitol and measuring the consequent changes in local curvature (see Experimental Procedures) (Misra et al., 2013). This assay showed that the OSW behaves as an elastic material whose surface modulus is approximately 2.3 times larger than that of the inner cell wall, yielding a bulk modulus 30 times larger (Figures 3E and 3F; Experimental Procedures). These properties remained nearly constant even after rupture (Figure 3F). Thus, the OSW is much stiffer than the inner/vegetative cell wall.

The presence of this rigid structure encasing the spore may influence growth, by reducing the effective stress generated by internal turgor pressure on the remodeling inner wall (Minc et al., 2009a). To test this, we reduced turgor by changing external osmolarity in a *gpd1Δ* mutant, which impairs osmoadaptation and found that this led to a significant reduction in growth rate, suggesting that growth in spores is powered by internal turgor as in vegetative cells (Minc et al., 2009a) (Figure 3G). We note that the simplest model for pressure-driven growth in walled cells predicts that growth rates are proportional to the surface modulus of the wall (Minc et al., 2009a). The changes in growth rate at outgrowth (increase by a factor 2.4; Figure S1B) are indeed comparable to the ratio between OSW and inner/vegetative cell-wall surface moduli ($\sigma_o/\sigma_i \approx 2.3$). Thus, these data suggest that the OSW may act as a mechanical barrier that slows down growth.

A Computational Model Reproduces Spore Morphogenesis and Predicts Variations in Outgrowth Onset with Changes in Wall Mechanics

Because the OSW is not majorly remodeled during spore development and behaves as an elastic material, it may accumulate elastic strain (equivalently mechanical stress) as the spore volume increases. As for most materials, the OSW may rupture if this strain exceeds a threshold that corresponds to the local failure stress (also known as ultimate strength of the material), and the volume increase needed to rupture it at outgrowth may relate to this threshold in strain (Figure 4A). To test this hypothesis, we developed numerical simulations of growing spores, using the following assumptions: (1) growth is powered by turgor pressure, (2) the inner wall is viscoelastic over the polarity cap because of remodeling, and elastic outside the cap (Minc et al., 2009a), (3) the OSW is elastic but may rupture when elastic strain (equivalently mechanical stress) exceeds a threshold, and (4) the cap center undergoes a random walk, which we use as a proxy for cap wandering by successive assembly/disassembly (Figure 4A; Supplemental Model). In simulations, we observed that spores remained roughly spherical until the OSW ruptured at a specific location, after which a polar tube began to elongate (Figures 4B and S5A; Movies S6 and S8). Starting from various initial conditions (n = 50 simulations), we found that the OSW ruptured when the ratio of spore volume to initial volume exceeded a well-defined threshold, thus reproducing experimental behavior (Figure 4C). In the model, this outgrowth threshold increased with the elastic strain (equivalently mechanical stress) threshold for OSW rupture and with the ratio of elastic moduli between OSW and inner wall (Figures 4D and S5B).

Mutants with Defective Spore Wall Hasten Outgrowth

A direct prediction of this mechanical model is that spores with defective spore wall structure or mechanical properties should outgrow at smaller volume ratio than wild-type spores. To test these aspects, we characterized spore wall mechanics and spore development in two mutants specifically defective in spore wall synthesis: *mok13Δ*, a mutant in an α-glucan synthase (García et al., 2006) and *chs1Δ*, a mutant in a chitin synthase (Arellano et al., 2000). These mutants depicted a marked reduction in the surface modulus of the OSW but no major difference in inner wall mechanics (Figure 4E), and indeed did outgrow at volume ratios that were significantly lower than WT: $< V_O/ V_G > = 1.46 \pm 0.10$ (n = 58) for *mok13Δ* and $< V_O/ V_G > = 1.57 \pm 0.11$ (n = 36) for *chs1Δ* (Figure 4F). This suggests that OSW mechanical properties contribute to the timing of outgrowth.

A Single Polar Cap Is Required for Singular Rupture in the OSW

An additional prediction of the model is that the threshold for rupture at outgrowth is first attained at the polar cap location, because mechanical stress in the OSW is enhanced by local growth (Figure 4A). Accordingly, simulations predicted that the OSW should rupture at many sites if growth is diffuse and not restricted to a single cap (Figure 5A). To experimentally test this, we assayed spores of the *orb6-25* mutant, a mutant in the NDR kinase orb6p, which shuts off polarity establishment at a downstream level when grown at restrictive temperature (Das et al., 2009). These spores grew in a perfectly isotropic manner, with polarity factors diffusely distributed around the surface, and remained round many hours after the typical timing corresponding to WT outgrowth (Figures 5B and 5C). We then performed TEM at different time points and indeed observed that, 6 hr after germination, this mutant presented multiple sites of spore wall rupture (Figure 5D). The number and size of holes in the OSW increased over time, as in the simulations (Figures 5E and S5D). Initial opening of the OSW in this mutant appeared at a volume ratio of $< V_{OSW\ opening}/V_G > = 2.18 \pm 0.40$ (n = 24), slightly higher than WT (Figure S5C).

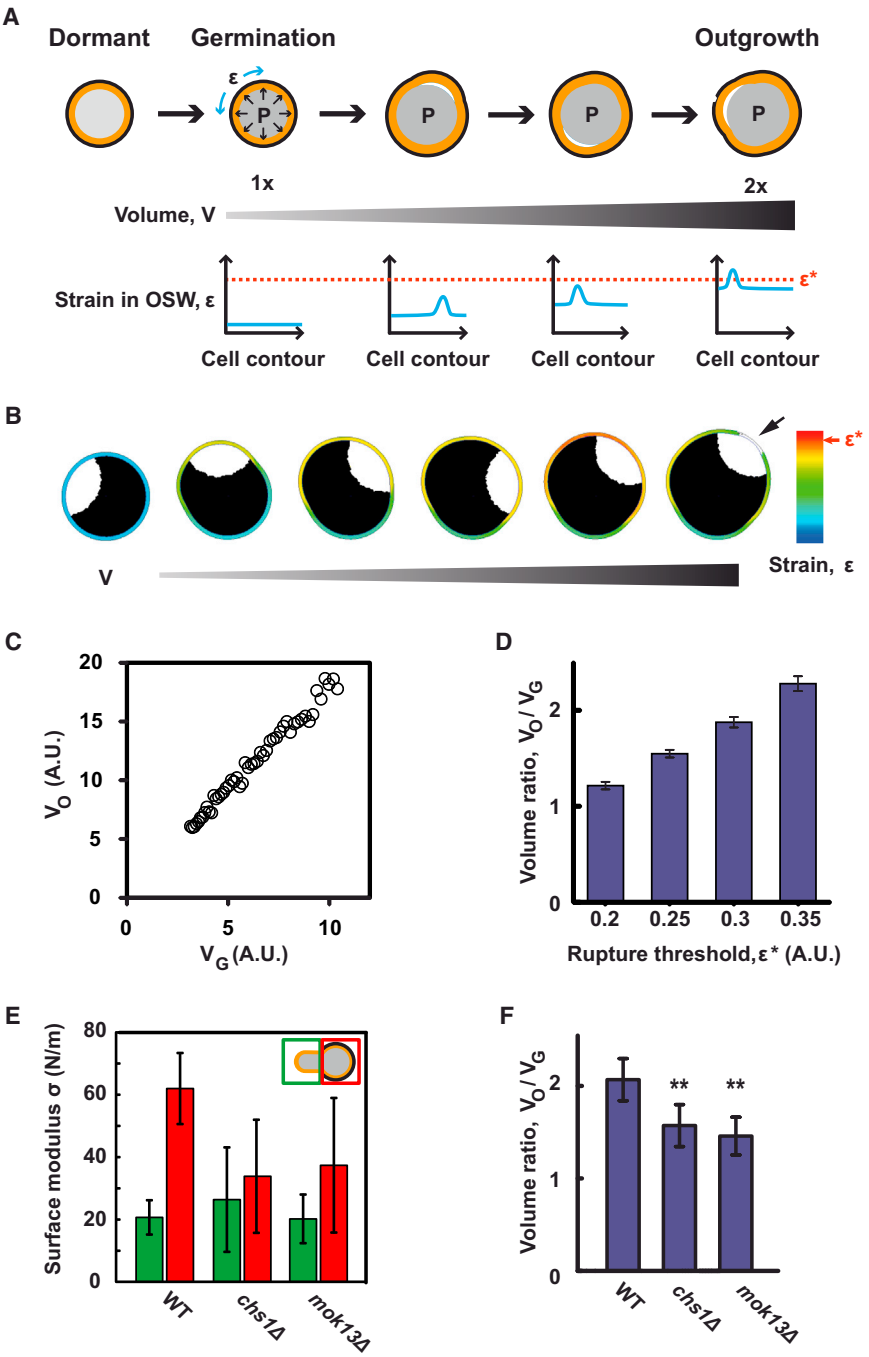

Figure 4. A Mechanical Model of Stress in the Outer Spore Wall Predicts Size-Increase Threshold for Wall Rupture and Outgrowth

(A) Schematic representing the geometry and inputs of the mechanical model. The spore grows under pressure, and is enclosed within the inner wall (orange) and the OSW (black). Growth is restricted to the polar cap. The OSW is under elastic strain ε, which increases globally as the spore grows, and locally at sites of polarized growth. The OSW ruptures above an elastic strain threshold ε^* corresponding to the failure stress of the material.

(B) Spores growing in silico. Colors in the OSW correspond to local strain values. Elastic moduli are assumed to be constant, and therefore the color code for strain also indicates the stress in the OSW.

(C) Theoretical prediction of volume doubling at outgrowth for a specific value of the threshold for rupture (n = 50 simulations).

(D) Dependence of volume ratio on the rupture threshold.

(E) Surface moduli for the walls on the spore (red bars) and cell (green bars) sides in outgrown spores of WT and *chs1Δ* and *mok13Δ* mutants (n > 10 spores for each condition).

(F) Volume ratios between outgrowth and germination for WT, *chs1Δ*, and *mok13Δ* mutants (n > 30 spores for each condition). Error bars represent SDs.

**p < 0.01, Student's t test. See also Figure S5 and Movie S6.

Thus, our mechanical model can predict both temporal and spatial rupture in the OSW at outgrowth and suggests a picture in which local growth at the cap locally increases the stress in the OSW until the failure stress is reached and the OSW ruptures (Figure 4A).

Local Laser-Induced Fragilization of the OSW Is Sufficient to Trigger Polar Cap Stabilization and Outgrowth

We next asked if the rupture in the OSW at outgrowth could influence polar cap stabilization. To directly assess this hypothesis, we developed a UV-laser assay to weaken the OSW with an intense pulse concentrated at a diffraction-limited spot on the spore surface. We optimized this assay to selectively weaken the OSW but not the inner wall (Figures S4B, S5E, and S5F; Experimental Procedures). We then filmed spores expressing GFP-bgs4 at early time points after germination and ablated the OSW either away from the polarity cap or at its exact location. Strikingly, the fragilization of the OSW at the cap caused it to stabilize and promoted the extension of a polarized tube at timings and volumes much smaller than in control nonablated spores in the same field of view (Figures 6A and 6B; Movie S7). Importantly, this effect was likely due to the mechanical fragilization of the OSW and not to a stress-activated recruitment or stabilization of polarity components (Kono et al., 2012). Spores ablated away from the cap did not show obvious recruitment at ablation sites and kept on wandering to stabilize at an independent location at similar timing and volumes as nonablated controls. These data suggest that the OSW has destabilizing effects on polarity, and that rupturing the OSW is sufficient to trigger cap stabilization and outgrowth.

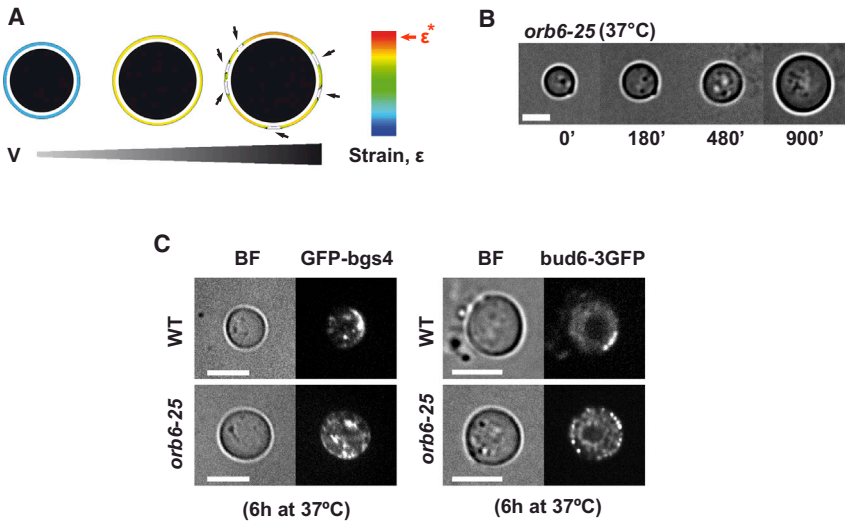

Figure 5. Polar Cap Assembly Is Required for Singular Rupture in the Spore Wall at Outgrowth

(A) Numerical simulations predicting multiple sites of rupture in spores with diffuse polarity.

(B) Time-lapse bright-field images of spore development in an *orb6-25* mutant grown at restrictive temperature (37°C) (scale bars, 5 μm).

(C) Single confocal midslices of WT and *orb6-25* spores expressing the polarity markers GFP-bgs4 or bud6-3GFP, 6 hr after germination at 37°C (scale bars, 5 μm).

(D) TEM of an *orb6-25* mutant spore 6 hr after germination at 37°C (scale bars, 1 μm) and close-up (scale bars, 200 nm). The black arrows point at sites of OSW ruptures.

(E) Quantification of phenotypes of OSW rupture at different times after germination at 37°C (n = 65 spores).

See also Figure S5.

A Positive Feedback between Growth and Polarity Can Account for the Switch in Polar Cap Stability at Outgrowth

To understand how the changes in the OSW could impact changes in polarity behavior, we turned to our numerical simulations to assess different hypotheses of feedbacks on polarity. We biased the random walk of the polar cap toward a location determined by (1) minimal stress, (2) maximal curvature, or (3) maximal surface expansion rate. Although all three hypotheses seem to be qualitatively in agreement with experimental observations, we found that with hypothesis (1) the cap does not stop wandering, whereas with hypothesis (2) the tube is immediately curved. Only hypothesis (3) reproduced observations, yielding the most robust behavior after outgrowth (Figures 7A and 7B; Movie S8). These modeling results thus suggest that a feedback from surface growth on the position of the polarity cap can explain polar cap stabilization at outgrowth.

To experimentally validate this prediction, we halted growth either by depolymerizing actin with Latrunculin A or by confining the growth of single spores in round microchambers. In these experiments, the controls (spores treated with DMSO or in large microchambers) displayed cap wandering and then stabilized, whereas the caps in nongrowing spores kept on wandering for several hours passed the timing of outgrowth in the control, exhibiting a marked increase in the number of unstable caps (Figures 7C and 7D). Thus, growth is required for cap stabilization. Furthermore, the coordinated OSW rupture and cap stabilization at outgrowth may be accounted for by a positive-feedback loop between growth and polarity, in which the cap promotes local growth while being preferentially stabilized at regions with higher surface growth rate.

DISCUSSION

By dynamically studying the developmental polarity and morphogenesis of single fission yeast spores, we develop and test here a simple quantitative model linking changes in the OSW with the spatial stability of polar caps needed for outgrowth. We propose that the OSW acts as a mechanical barrier, which hinders growth and destabilizes polarity. A rupture in this barrier generated by local polar growth when spores have grown enough releases inhibition by the OSW, stabilizes the cap, and coordinates spatial and temporal aspects of outgrowth. Instead of sensing absolute size (Turner et al., 2012), outgrowth appears to be triggered upon a fold change in volume. A function of this sensing system might be to prevent the reorganizing spores to exit the spore protective shell too early, as well as to regulate the timing and cell sizing at outgrowth in the absence of a tight cell-cycle regulation (Hatanaka and Shimoda, 2001). Through modeling and experimental tests, we demonstrate that a positive feedback between growth and polarity can account for a switch from unstable to stable polar cap behavior. Spatial landmarks from previous cell cycles, or MT-based targeting do not appear to be required at these early stages. MTs are also dispensable for de novo tip growth in rounded fission yeast spheroplasts or in mutants branching from cell sides (Kelly and Nurse, 2011; Sawin and Snaith, 2004). In addition, many cellular systems display transient oscillation of polar caps, which then stabilize at a fixed position even in the absence of directional cues (Bendezú and Martin, 2013; Dyer et al., 2013).

Polarity Cap Oscillations

The initial polarity cap establishment in these spores is likely to involve an interplay between reaction-diffusion-based positive and negative feedbacks that promote the self-assembly of a

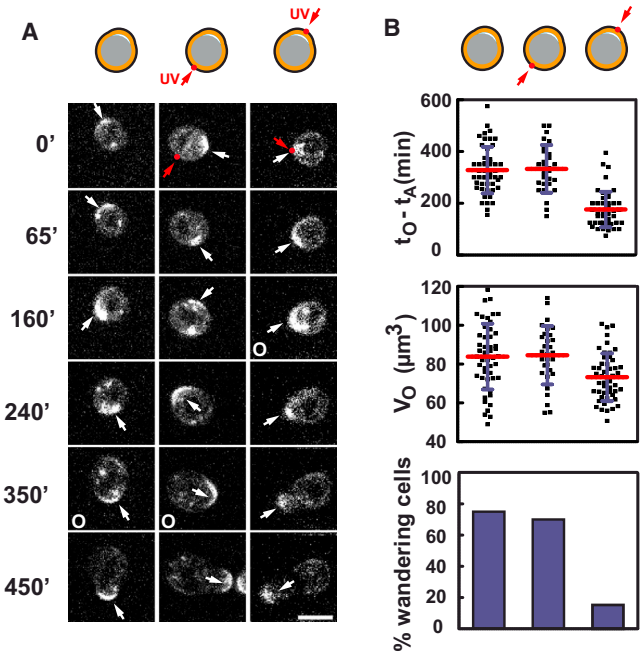

Figure 6. Rupturing the Outer Spore Wall Is Sufficient to Spatially Stabilize the Polar Cap

(A) Time-lapse single confocal midslices of germinating spores expressing GFP-bgs4 in the following conditions: not photoablated, photoablated away from the cap, and photoablated at the cap location with a UV laser. White arrows point at polar cap positions, and red arrows and dots indicate the photoablation site.

(B) Time of outgrowth with reference to laser irradiation, absolute volume at outgrowth, and percentage of spores depicting cap oscillations in the 2 hr following laser irradiation for the same three conditions as in (A).

Red bars: mean values; blue bars: SDs. Scale bars, 5 μm. See also Figure S5 and Movie S7.

single front of active-cdc42p (Bendezú and Martin, 2012; Das et al., 2012; Wu and Lew, 2013). We found that actin-based transport was not required in spores, although we note that actin inhibition caused a reduction in cap size (Figure S3B). The observed cap oscillations could be by-products of intrinsic mechanisms of polarization systems (Bendezú and Martin, 2012; Wu and Lew, 2013). Alternatively, they may function as a search mechanism when polarity needs to be redirected (Bendezú and Martin, 2013). In spores, the stochastic wandering of the cap could serve to identify a "weak spot" in the spore wall. Although our inspection of electron microscopy images of the OSW in fission yeast did not reveal obvious opening in the OSW in dormant spores (Figures 3A and S4A), certain fungal species display germ pores, which are small defects in the OSW from which the polar tube may emerge (Walkinshaw et al., 1967). Similarly, pollen tubes exit from specific apertures in the walls of pollen grains (Furness and Rudall, 2004) and early embryos of the marine brown algae *Fucus* use cues from the cell wall for polarity and outgrowth (Quatrano and Shaw, 1997). Our mechanism, whereby polar cap stability is amplified by growth, could serve to explain how these cells may polarize using mechanical cues from the cell wall.

Crosstalks between Growth and Polarity

Our work directly evidences the requirement of growth to spatially stabilize a polarity front. Similar growth-polarity feedbacks have been recently proposed in plants to regulate auxin-driven patterning of the shoot apex (Nakayama et al., 2012). Different tip-growing walled cells display variation in elongation rate that can range over almost two orders of magnitude (Knechtle et al., 2003; Qin and Yang, 2011). It is thus plausible that they have evolved mechanisms to monitor growth rate and link it to polarity machineries. A failure to do so could yield deleterious variations in cell-wall thickness and risks of cell death by bursting, or growth arrest (Campàs and Mahadevan, 2009). These growth-polarity feedbacks may underlie switching behavior such as oscillatory growth and contact sensing seen in fungal hyphae and pollen tubes (Kumamoto and Vinces, 2005; Qin and Yang, 2011; Rojas et al., 2011). Recent work in *S. cerevisiae* suggests models by which transport and fusion of vesicles may dilute polarity caps thereby causing them to disassemble (Layton et al., 2011). A reduction of surface expansion rate would yield similar dilution effects at a constant vesicle flux, and destabilize polarity. Conversely, the constraining effect of the OSW on surface expansion could restrict the available space needed for sufficient new membrane or inner wall addition necessary to stabilize the polar cap. In addition, we speculate that growth rates could impact polarity stability through a differential monitoring of cellular dimensions by intracellular gradients (Howard, 2012; Moseley and Nurse, 2010). Further work will be needed to fully characterize complex interplays between these essential morphogenetic cellular parameters.

Mechanochemical Coupling in Cell Polarity

Our data in conjunction with others support the existence of self-organizing processes coupling surface mechanics, growth, and internal organization. In animal cells, the micromechanical property of the actin cortex has been proposed to act as an important element to control polarity and shape changes during migration or cytokinesis (Paluch et al., 2006; Salbreux et al., 2012; Sedzinski et al., 2011). In addition, recent studies in migrating neutrophils suggest that membrane tension may have global inhibitory effects on polarity that function to maintain a singular active domain at the cell front (Houk et al., 2012). Thus, our work adds to a growing appreciation of mechanochemical feedbacks that serve to pattern cell shape and polarity (Asnacios and Hamant, 2012; Howard et al., 2011). The steady-state morphogenesis of a cell, like the rod shape of fission yeast, is likely to involve many types of feedbacks (Minc et al., 2009b; Terenna et al., 2008), which cannot be dissected with genetics. Thus, in addition to large-scale studies of gene products regulating cell shape and polarity (Hayles et al., 2013), dynamic studies like the one we performed here promise to pave the way for integrated models of morphogenesis.

EXPERIMENTAL PROCEDURES

Yeast Strains, Media, and Genetic Methods

Standard methods for *S. pombe* media and genetic manipulations were used (http://www-bcf.usc.edu/~forsburg/). Strains used in this study are

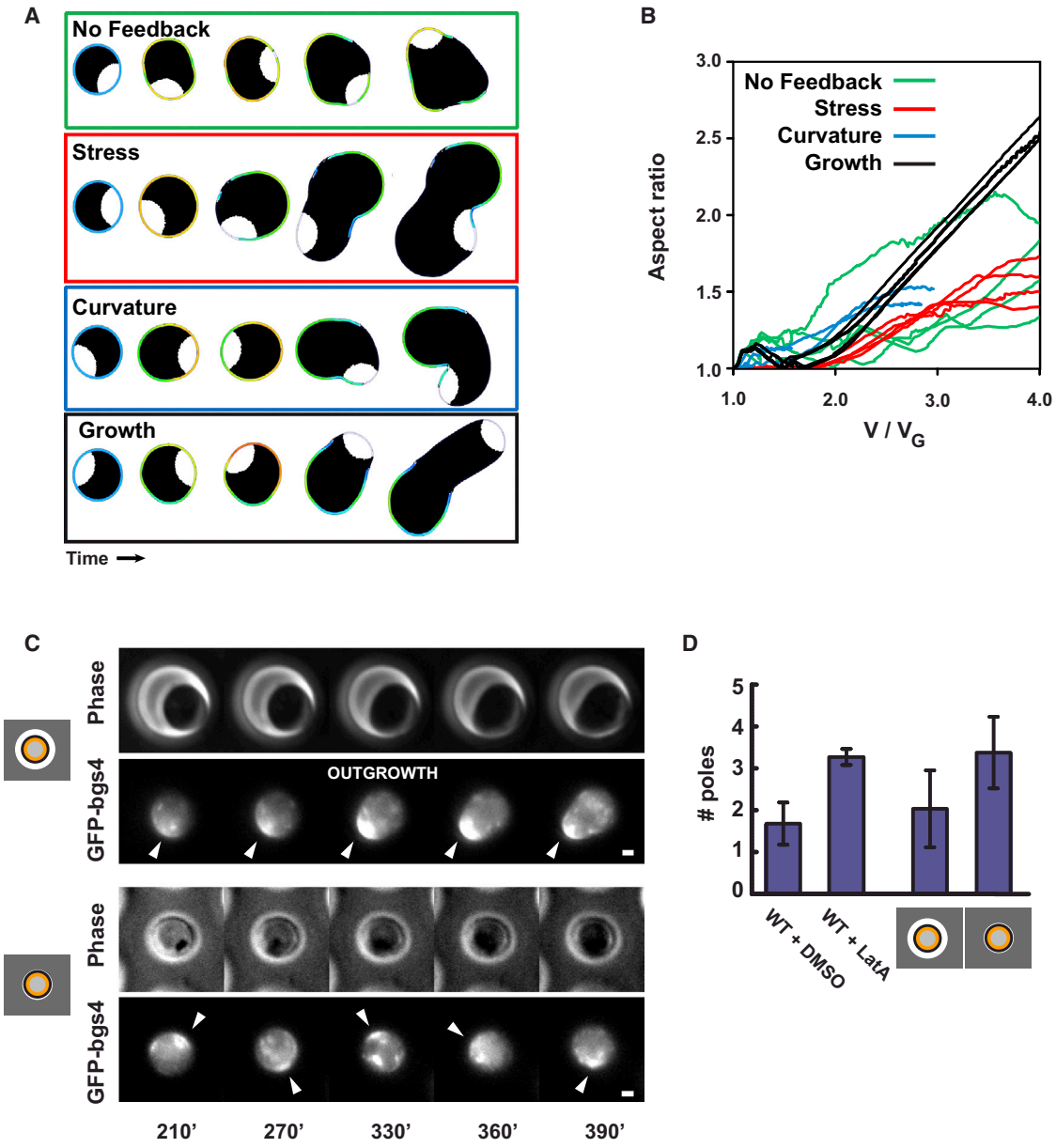

Figure 7. Outgrowth Involves a Positive-Feedback Loop between Growth and Polarity

(A) Numerical simulations testing different sources of feedback for polarity stabilization at outgrowth: no feedback, feedback on minimal mechanical stress, feedback on maximal curvature, feedback on maximal surface expansion rate (growth).

(B) Model prediction for the evolution of the aspect ratio as a function of normalized volume in the same conditions as in (A).

(C) Epifluorescence time-lapse of germinating spores expressing GFP-bgs4 arising from the same population, placed in large (on top) or small confining (on bottom) PDMS microchambers. White arrows point at successive polarity cap positions.

(D) Total number of observed successive polar caps for spores expressing CRIB-GFP treated with DMSO or 100 μM of Latrunculin A, which halts growth, and for spores expressing GFP-bgs4 in large or confining microchambers (n > 15 spores for each condition). Error bars represent SDs.

Scale bars, 1 μm. See also Movie S8.

listed in Table S1. Spores were obtained from homothallic h90 strains, or from diploids when indicated. Freshly growing cells were sporulated on malt extract (ME) solid media for 3 days. Spores were then digested 1 hr at room temperature in 1/200 glusulase solution in water to kill vegetative cells, and the enzyme was washed out three times in water. Digestion with glusulase did not influence morphogenetic and polarity events (size sensing and cap wandering) described in the manuscript (data not shown).

Pharmacological Inhibitors

Methyl-2-benzimidazole carbamate (MBC, Sigma) was used at a final concentration of 50 μg/ml from a 100× stock solution made fresh in DMSO. Latrunculin A (LatA, Sigma) was used at a final concentration of 100 μM from a 100× stock in DMSO. The efficiency of these treatments in rapidly depolymerizing microtubules and actin, respectively, was assessed by treating a mixed population of spores and cells for 10 min and imaging atb2-GFP for microtubules and the actin patch marker crn1-GFP (Figures S3C and S3D).

Microscopy

For long-term imaging, spores in water solution were placed on 2% agar YE5S pads and covered with a coverslip. For some applications, spores were placed in microfluidic chambers between a dialysis membrane and a coverslip, which allowed live fluid exchange (Charvin et al., 2008). Spore development was imaged at room temperature (23°C–25°C), with controlled humidity, with an inverted epifluorescence microscope provided with a motorized stage and automatic focus (Nikon Ti-Eclipse), and an EM-CCD camera (Hamamatsu). Movies were generally acquired at 100× magnification with 5 or 10 min time intervals, using phase contrast and epifluorescence when necessary. GFP-tagged polarity markers were also imaged with a spinning-disk confocal fluorescent microscope (Yokagawa, CSU-X1 spinning head) equipped with an EM-CCD camera (Evolve, Photometrics) and a 100× oil immersion objective (Nikon S Fluor 100× 0.5–1.3 NA). Images were acquired with Micromanager or Metamorph and processed and analyzed with Image J and MATLAB (MathWorks).

Image Analysis

Morphogenetic parameters of single developing spores were extracted from phase-contrast time-lapses using home-built MATLAB scripts (available upon request). Cell contours were segmented from the phase images, at each time point and oriented along the future outgrowth axis, yielding the morphogenesis color plots depicted in Figure 1B. The precision in contour segmentation was calibrated using spores expressing a plasma membrane marker GFP-psy1. The long axis was identified at each time point, and the aspect ratio was computed as the ratio between the length along this axis and the largest perpendicular diameter. Volumes were computed by assuming a prolate geometry (rotational symmetry around the long axis of the cell). The long axis was thus sliced in local diameters y(x) every pixel (Figure 1B, inset) which served to compute the areas of the sections of the prolate $S(x) = \pi^*(y(x)/2)^2$, and the volume was computed as the sum of these areas along all the pixels of the long axis. We estimate imprecisions associated to these methods (including errors in the z, segmentation, and prolate approximation), to be lower than 5% for length and aspect ratio and on the order of 10% for the volume.

The frequency of new caps during the initial phase of near-isotropic growth (Figures 2C and 2E) was visually quantified from time-lapse epifluorescence movies of cells expressing GFP-bgs4. Only fully reassembling new caps were counted, and the number of caps was divided by the time between first cap appearance and outgrowth. The last stable cap-promoting outgrowth was not counted.

Quantification of relative concentration evolution of polarity factors at the cap (Figure 2F) was inferred from computing the mean signal at the polar cap from a merged confocal stack of six z-sections time-lapsed on individual spores. Growing spores were imaged together with vegetative cells, to normalize the concentration in spore caps with the concentration in vegetative bipolar caps. Photobleaching was accounted for by quantifying the loss of signal in fixed cells expressing the same marker, and autofluorescence was accounted for by imaging WT spores and cells with no marker.

Transmission Electron Microscopy

Wild-type spores were grown in liquid YE5S at 30°C for different amounts of time and subsequently fixed in 2% glutaraldehyde in YE5S for 30 min on ice. *orb6-25* mutants spores were grown at 37°C for different amounts of times and fixed in same conditions. Spores were then transferred to 0.1 M PBS + 2% glutaraldehyde and stirred overnight at 4°C. The spore pellet was then dehydrated in ethanol and embedded in Epon resine. Ultrathin sections were made with an ultramicrotome (Leica), deposited onto electron microscopy grids, and contrasted with uranyl acetate in lead citrate. Images were taken using a FEI CM120 electron microscope (FEI Company), equipped with a numeric camera (Keen View; Soft Imaging System, SIS).

Laser Ablation of the Outer Spore Wall

The laser ablation assay uses a pulsed 355 nm ultraviolet laser interfaced with an iLas system (Roper Scientific) in the "Mosquito" mode. This allows irradiating at multiple positions in the field with laser spots having a fixed area of about 500 nm. This system is mounted on a confocal spinning disk (Yokagawa CSU-X1 spinning head on a Nikon Eclipse Ti inverted microscope) equipped with an EM-CCD camera (Evolve, Photometrics) and a 100× oil immersion objective (Nikon S Fluor 100× 0.5–1.3 NA). We calibrated the irradiation time to optimize the selectivity of the assay in fragilizing the spore wall but not the inner wall. To this aim, spores were placed in microfluidic flow chambers, irradiated, and subsequently rinsed with a mix of two vegetative cell-wall (inner wall) digestion enzymes (0.5 mg/ml Zymolase and 10 mg/ml Novozyme). Rinsing with these enzymes yields the death of all vegetative cells and outgrown spores in 10–30 min but does not affect spores (Figure S4B). Using this assay, we identified the laser time of exposure that did not yield spore death without enzyme treatment, but that yielded death of irradiated spores after enzyme treatment. The optimal exposure time in our conditions was found to be 80 ms. The photoablation assay as presented in Figure 6 was then performed in these same conditions on spores expressing the polarity marker GFP-bgs4, that were germinated in YE5S liquid for 3 hr before laser irradiation.

Stress-Strain Experiment to Measure Rigidity of the OSW and Inner Cell Wall

To compute surface moduli of cell walls, spores, outgrown spores, and vegetative cells were placed in microfluidic chambers in YE5S media. The media was then exchanged rapidly and replaced by YE5S with a given concentration of sorbitol. This created a relative change in the internal osmotic pressure computed as $\Delta p = C_s RT$, with C_s the sorbitol concentration, R the gas constant, and T the temperature. This change in osmolarity caused the spores and cells to shrink, which serves as a measure of strain. Local changes in curvature radii, r, (before and 5 min after treatment) were tracked using homemade MATLAB scripts (Figure 3E). This assay was then repeated with dose-dependent addition of sorbitol (C_s = 2 M, 1.5 M, 1 M, 0.5 M), which allowed us to derive a stress-strain curve (Figure S4C). This curve was found to be linear within the regime probed, which reflects elastic behavior of both inner and outer spore wall, on short timescales. The slopes were then extracted to compute the average surface moduli of spores, using the following formula:

$$\frac{\Delta P}{\Delta r} = 4\frac{\sigma}{r^2}$$

This assay was used to derive average surface moduli of spores, vegetative cells, the back of outgrown spores (where the OSW is still encasing the inner wall) and the tip of outgrown spores (which only have vegetative wall) (Figure 3E). In vegetative cells, this analysis led to a value of the surface modulus of the cell wall of $\sigma_{Veg} = 18.6\ N.m^{-1}$, which closely agrees with measurement achieved by other means (Minc et al., 2009a). The surface modulus of the back of the spores was found to be $\sigma_{back} = 62.0\ N.m^{-1}$, and the surface modulus at the tip of the emerging tube was very close to the vegetative value: $\sigma_{tip} = 20.6\ N.m^{-1}$. Because the back of the spore has superimposed inner and outer wall, $\sigma_{back} = \sigma_i + \sigma_o$, whereas $\sigma_{tip} = \sigma_i$. Thus, the ratio between the surface moduli of the outer and the inner wall can be computed from $\sigma_o/\sigma_i = \sigma_{back}/\sigma_{tip} - 1 \approx 2.3$. Because the thickness, h_0, of the outer wall is approximately 15 nm and the thickness of the inner wall, h_i, is around 200 nm, the ratio in bulk moduli $E_o/E_i = (h_O\sigma_o)/(h_i\sigma_i)$ is around 30. The same assay and analysis were then used to characterize rigidity of spore walls in *chs1Δ* and *mok13Δ* mutants defective in spore wall synthesis (Figure 4E).

Assessment of the Role of Turgor Pressure in Spore Growth

Spores of either WT or *gpd1Δ* were first germinated and grown at 30°C for 2 hr in liquid YE5S. Spores were then placed in microfluidic chambers and covered with a semipermeable dialysis membrane. Single spore growth rates were monitored from time-lapse imaging during 2 hr, after which the spores were rinsed with 1 M sorbitol to decrease internal turgor, and growth rates were measured again for another 2 hr. Growth rate ratio before and after treatment was then computed for each single spore and averaged to plot the bar graph presented in Figure 3F.

Microchambers Operation

Microchambers were fabricated by the use of standard soft-lithography methods (Minc et al., 2009a, 2009b). Chambers are round, are 3–4 μm deep, and have diameters varying between 3 and 10 μm. Spores expressing the polarity marker GFP-bgs4 were germinated and grown for 3 hr 30 min, and a

1 μl drop of spore suspension was then placed at the bottom of a round fluorodish (WPI). The polydimethylsiloxane (PDMS) block containing the chambers was activated with a plasma cleaner and subsequently placed, holes facing down, on top of the spores in the dish and let to bind to the glass bottom. This forced many spores into single microchambers, some constraining, and some much larger than the spore diameter, that were used as controls. Time-lapses at different positions were then recorded to monitor polar cap wandering in different conditions.

SUPPLEMENTAL INFORMATION

Supplemental Information includes supplemental model, five figures, one table, and eight movies and can be found with this article online at http://dx.doi.org/10.1016/j.devcel.2014.01.023.

ACKNOWLEDGMENTS

We thank the Coudreuse, Martin, Perez, Ribas, Valdivieso, Sanchez, Chang, Tran, and Paoletti labs for sharing strains and materials. D.B. was supported by an Institut Curie PhD fellowship in the initial period of this work. A.B. is supported by a European Research Council starting grant (PhyMorph, #307387). N.M. acknowledges support from CNRS, FP7 (CIG and ITN programs), ANR (grant 10PDOC00301), FRM (grant AJE20130426890), and a Mairie de Paris "Emergence grant."

Received: September 24, 2013
Revised: January 6, 2014
Accepted: January 23, 2014
Published: March 10, 2014

REFERENCES

Arellano, M., Cartagena-Lirola, H., Nasser Hajibagheri, M.A., Durán, A., and Henar Valdivieso, M. (2000). Proper ascospore maturation requires the chs1+ chitin synthase gene in Schizosaccharomyces pombe. Mol. Microbiol. *35*, 79–89.

Asnacios, A., and Hamant, O. (2012). The mechanics behind cell polarity. Trends Cell Biol. *22*, 584–591.

Bastmeyer, M., Deising, H.B., and Bechinger, C. (2002). Force exertion in fungal infection. Annu. Rev. Biophys. Biomol. Struct. *31*, 321–341.

Bendezú, F.O., and Martin, S.G. (2012). Cdc42 oscillations in yeasts. Sci. Signal. *5*, pe53.

Bendezú, F.O., and Martin, S.G. (2013). Cdc42 explores the cell periphery for mate selection in fission yeast. Curr. Biol. *23*, 42–47.

Boudaoud, A. (2003). Growth of walled cells: from shells to vesicles. Phys. Rev. Lett. *91*, 018104.

Campàs, O., and Mahadevan, L. (2009). Shape and dynamics of tip-growing cells. Curr. Biol. *19*, 2102–2107.

Cano, R.J., and Borucki, M.K. (1995). Revival and identification of bacterial spores in 25- to 40-million-year-old Dominican amber. Science *268*, 1060–1064.

Chang, F., and Martin, S.G. (2009). Shaping fission yeast with microtubules. Cold Spring Harb. Perspect. Biol. *1*, a001347.

Charvin, G., Cross, F.R., and Siggia, E.D. (2008). A microfluidic device for temporally controlled gene expression and long-term fluorescent imaging in unperturbed dividing yeast cells. PLoS ONE *3*, e1468.

Cortés, J.C., Carnero, E., Ishiguro, J., Sánchez, Y., Durán, A., and Ribas, J.C. (2005). The novel fission yeast (1,3)beta-D-glucan synthase catalytic subunit Bgs4p is essential during both cytokinesis and polarized growth. J. Cell Sci. *118*, 157–174.

Das, M., Wiley, D.J., Medina, S., Vincent, H.A., Larrea, M., Oriolo, A., and Verde, F. (2007). Regulation of cell diameter, For3p localization, and cell symmetry by fission yeast Rho-GAP Rga4p. Mol. Biol. Cell *18*, 2090–2101.

Das, M., Wiley, D.J., Chen, X., Shah, K., and Verde, F. (2009). The conserved NDR kinase Orb6 controls polarized cell growth by spatial regulation of the small GTPase Cdc42. Curr. Biol. *19*, 1314–1319.

Das, M., Drake, T., Wiley, D.J., Buchwald, P., Vavylonis, D., and Verde, F. (2012). Oscillatory dynamics of Cdc42 GTPase in the control of polarized growth. Science *337*, 239–243.

Drubin, D.G. (1991). Development of cell polarity in budding yeast. Cell *65*, 1093–1096.

Dyer, J.M., Savage, N.S., Jin, M., Zyla, T.R., Elston, T.C., and Lew, D.J. (2013). Tracking shallow chemical gradients by actin-driven wandering of the polarization site. Curr. Biol. *23*, 32–41.

Fink, J., Carpi, N., Betz, T., Bétard, A., Chebah, M., Azioune, A., Bornens, M., Sykes, C., Fetler, L., Cuvelier, D., and Piel, M. (2011). External forces control mitotic spindle positioning. Nat. Cell Biol. *13*, 771–778.

Furness, C.A., and Rudall, P.J. (2004). Pollen aperture evolution—a crucial factor for eudicot success? Trends Plant Sci. *9*, 154–158.

García, I., Tajadura, V., Martín, V., Toda, T., and Sánchez, Y. (2006). Synthesis of alpha-glucans in fission yeast spores is carried out by three alpha-glucan synthase paralogues, Mok12p, Mok13p and Mok14p. Mol. Microbiol. *59*, 836–853.

Glynn, J.M., Lustig, R.J., Berlin, A., and Chang, F. (2001). Role of bud6p and tea1p in the interaction between actin and microtubules for the establishment of cell polarity in fission yeast. Curr. Biol. *11*, 836–845.

Harold, F.M. (1990). To shape a cell: an inquiry into the causes of morphogenesis of microorganisms. Microbiol. Rev. *54*, 381–431.

Hatanaka, M., and Shimoda, C. (2001). The cyclic AMP/PKA signal pathway is required for initiation of spore germination in Schizosaccharomyces pombe. Yeast *18*, 207–217.

Hayles, J., Wood, V., Jeffery, L., Hoe, K.L., Kim, D.U., Park, H.O., Salas-Pino, S., Heichinger, C., and Nurse, P. (2013). A genome-wide resource of cell cycle and cell shape genes of fission yeast. Open Biol. *3*, 130053.

Houk, A.R., Jilkine, A., Mejean, C.O., Boltyanskiy, R., Dufresne, E.R., Angenent, S.B., Altschuler, S.J., Wu, L.F., and Weiner, O.D. (2012). Membrane tension maintains cell polarity by confining signals to the leading edge during neutrophil migration. Cell *148*, 175–188.

Howard, M. (2012). How to build a robust intracellular concentration gradient. Trends Cell Biol. *22*, 311–317.

Howard, J., Grill, S.W., and Bois, J.S. (2011). Turing's next steps: the mechanochemical basis of morphogenesis. Nat. Rev. Mol. Cell Biol. *12*, 392–398.

Howell, A.S., Jin, M., Wu, C.F., Zyla, T.R., Elston, T.C., and Lew, D.J. (2012). Negative feedback enhances robustness in the yeast polarity establishment circuit. Cell *149*, 322–333.

Kelly, F.D., and Nurse, P. (2011). De novo growth zone formation from fission yeast spheroplasts. PLoS ONE *6*, e27977.

Klobutcher, L.A., Ragkousi, K., and Setlow, P. (2006). The Bacillus subtilis spore coat provides "eat resistance" during phagocytic predation by the protozoan Tetrahymena thermophila. Proc. Natl. Acad. Sci. USA *103*, 165–170.

Knechtle, P., Dietrich, F., and Philippsen, P. (2003). Maximal polar growth potential depends on the polarisome component AgSpa2 in the filamentous fungus Ashbya gossypii. Mol. Biol. Cell *14*, 4140–4154.

Kono, K., Matsunaga, R., Hirata, A., Suzuki, G., Abe, M., and Ohya, Y. (2005). Involvement of actin and polarisome in morphological change during spore germination of Saccharomyces cerevisiae. Yeast *22*, 129–139.

Kono, K., Saeki, Y., Yoshida, S., Tanaka, K., and Pellman, D. (2012). Proteasomal degradation resolves competition between cell polarization and cellular wound healing. Cell *150*, 151–164.

Kumamoto, C.A., and Vinces, M.D. (2005). Alternative Candida albicans lifestyles: growth on surfaces. Annu. Rev. Microbiol. *59*, 113–133.

Layton, A.T., Savage, N.S., Howell, A.S., Carroll, S.Y., Drubin, D.G., and Lew, D.J. (2011). Modeling vesicle traffic reveals unexpected consequences for Cdc42p-mediated polarity establishment. Curr. Biol. *21*, 184–194.

McKenney, P.T., Driks, A., and Eichenberger, P. (2013). The Bacillus subtilis endospore: assembly and functions of the multilayered coat. Nat. Rev. Microbiol. *11*, 33–44.

Minc, N., Boudaoud, A., and Chang, F. (2009a). Mechanical forces of fission yeast growth. Curr. Biol. *19*, 1096–1101.

Minc, N., Bratman, S.V., Basu, R., and Chang, F. (2009b). Establishing new sites of polarization by microtubules. Curr. Biol. *19*, 83–94.

Misra, G., Rojas, E.R., Gopinathan, A., and Huang, K.C. (2013). Mechanical consequences of cell-wall turnover in the elongation of a Gram-positive bacterium. Biophys. J. *104*, 2342–2352.

Mitchison, J.M., and Nurse, P. (1985). Growth in cell length in the fission yeast Schizosaccharomyces pombe. J. Cell Sci. *75*, 357–376.

Moseley, J.B., and Nurse, P. (2010). Cell division intersects with cell geometry. Cell *142*, 184–188.

Nakayama, N., Smith, R.S., Mandel, T., Robinson, S., Kimura, S., Boudaoud, A., and Kuhlemeier, C. (2012). Mechanical regulation of auxin-mediated growth. Curr. Biol. *22*, 1468–1476.

Neiman, A.M. (2005). Ascospore formation in the yeast Saccharomyces cerevisiae. Microbiol. Mol. Biol. Rev. *69*, 565–584.

Nurse, P., Thuriaux, P., and Nasmyth, K. (1976). Genetic control of the cell division cycle in the fission yeast Schizosaccharomyces pombe. Mol. Gen. Genet. *146*, 167–178.

Paluch, E., van der Gucht, J., and Sykes, C. (2006). Cracking up: symmetry breaking in cellular systems. J. Cell Biol. *175*, 687–692.

Pandey, R., Ter Beek, A., Vischer, N.O., Smelt, J.P., Brul, S., and Manders, E.M. (2013). Live cell imaging of germination and outgrowth of individual bacillus subtilis spores; the effect of heat stress quantitatively analyzed with SporeTracker. PLoS ONE *8*, e58972.

Qin, Y., and Yang, Z. (2011). Rapid tip growth: insights from pollen tubes. Semin. Cell Dev. Biol. *22*, 816–824.

Quatrano, R.S., and Shaw, S.L. (1997). Role of the cell wall in the determination of cell polarity and the plane of cell division in Fucus embryos. Trends Plant Sci. *2*, 15–21.

Rincón, S.A., Ye, Y., Villar-Tajadura, M.A., Santos, B., Martin, S.G., and Pérez, P. (2009). Pob1 participates in the Cdc42 regulation of fission yeast actin cytoskeleton. Mol. Biol. Cell *20*, 4390–4399.

Rojas, E.R., Hotton, S., and Dumais, J. (2011). Chemically mediated mechanical expansion of the pollen tube cell wall. Biophys. J. *101*, 1844–1853.

Salbreux, G., Charras, G., and Paluch, E. (2012). Actin cortex mechanics and cellular morphogenesis. Trends Cell Biol. *22*, 536–545.

Sawin, K.E., and Snaith, H.A. (2004). Role of microtubules and tea1p in establishment and maintenance of fission yeast cell polarity. J. Cell Sci. *117*, 689–700.

Sedzinski, J., Biro, M., Oswald, A., Tinevez, J.Y., Salbreux, G., and Paluch, E. (2011). Polar actomyosin contractility destabilizes the position of the cytokinetic furrow. Nature *476*, 462–466.

Slaughter, B., and Li, R. (2006). Toward a molecular interpretation of the surface stress theory for yeast morphogenesis. Curr. Opin. Cell Biol. *18*, 47–53.

Tanaka, K., and Hirata, A. (1982). Ascospore development in the fission yeasts Schizosaccharomyces pombe and S. japonicus. J. Cell Sci. *56*, 263–279.

Tatebe, H., Nakano, K., Maximo, R., and Shiozaki, K. (2008). Pom1 DYRK regulates localization of the Rga4 GAP to ensure bipolar activation of Cdc42 in fission yeast. Curr. Biol. *18*, 322–330.

Terenna, C.R., Makushok, T., Velve-Casquillas, G., Baigl, D., Chen, Y., Bornens, M., Paoletti, A., Piel, M., and Tran, P.T. (2008). Physical mechanisms redirecting cell polarity and cell shape in fission yeast. Curr. Biol. *18*, 1748–1753.

Turner, J.J., Ewald, J.C., and Skotheim, J.M. (2012). Cell size control in yeast. Curr. Biol. *22*, R350–R359.

Walkinshaw, C.H., Hyde, J.M., and van Zandt, J. (1967). Fine structure of quiescent and germinating aeciospores of Cronartium fusiforme. J. Bacteriol. *94*, 245–254.

Wallace, S., Fleming, A., Wellman, C.H., and Beerling, D.J. (2011). Evolutionary development of the plant and spore wall. AoB Plants *2011*, plr027.

Wedlich-Soldner, R., Altschuler, S., Wu, L., and Li, R. (2003). Spontaneous cell polarization through actomyosin-based delivery of the Cdc42 GTPase. Science *299*, 1231–1235.

Wu, C.F., and Lew, D.J. (2013). Beyond symmetry-breaking: competition and negative feedback in GTPase regulation. Trends Cell Biol. *23*, 476–483.